7-25-2017

Fracture Modeling of Lithium-Silicon Battery Based on Variable Elastic Moduli

Abhishek Sarkar
Iowa State University, asarkar@ameslab.gov

Pranav Shrotriya
Iowa State University, shrotriy@iastate.edu

Abhijit Chandra
Iowa State University, achandra@iastate.edu

Fracture Modeling of Lithium-Silicon Battery Based on Variable Elastic Moduli

Abstract

Mechanical stresses which develops during lithiation of crystalline silicon particles in lithium silicon battery causes fracture and limits the life of silicon based lithium batteries. We formulated an elasto-plastic stress formulation for a two-phase silicon model and investigated the influence of different mechanical properties of lithiated silicon on the fracture of nanoparticles during first cycle charging. A chemo-mechanical model was developed to determine lithium distribution and associated stress states during first cycle lithiation. The concentration gradient of lithium and an elastic perfectly plastic material behavior for silicon were considered to evaluate stress distribution formulation and determine stress field in the particle. The stress profile was used to perform a crack growth analysis. The stress distribution formulation was validated by evaluating stress field for different elastic modulus value for lithiated silicon and comparing our inference against observations from prior experiments. The results showed lower modulus of lithiated silicon yielded results like experimental observations for nanoparticles. The size dependent fracture behavior was also observed in lower elastic modulus of lithiated silicon. We conclude that accurate mechanical characterization of lithiated silicon nanoparticle is necessary to model the failure of silicon particle and improving the mechanical properties may suppress crack growth in silicon nanoparticles during charging.

Keywords

Elastic-Plastic Deformation, Fracture Mechanics, Lithium-ion Battery, Reactive Diffusion, Silicon

Disciplines

Electro-Mechanical Systems | Mechanical Engineering

Comments

This article is published as Sarkar, Abhishek, Pranav Shrotriya, and Abhijit Chandra. "Fracture modeling of lithium-silicon battery based on variable elastic moduli." *Journal of The Electrochemical Society* 164, no. 11 (2017): E3606-E3612. DOI: 10.1149/2.0631711jes. Posted with permission.

JES Focus Issue on Mathematical Modeling of Electrochemical Systems at Multiple Scales in Honor of John Newman

Fracture Modeling of Lithium-Silicon Battery Based on Variable Elastic Moduli

Abhishek Sarkar, Pranav Shrotriya,[z] and Abhijit Chandra

Department of Mechanical Engineering, Iowa State University, Ames, Iowa 50010, USA

Mechanical stresses which develops during lithiation of crystalline silicon particles in lithium silicon battery causes fracture and limits the life of silicon based lithium batteries. We formulated an elasto-plastic stress formulation for a two-phase silicon model and investigated the influence of different mechanical properties of lithiated silicon on the fracture of nanoparticles during first cycle charging. A chemo-mechanical model was developed to determine lithium distribution and associated stress states during first cycle lithiation. The concentration gradient of lithium and an elastic perfectly plastic material behavior for silicon were considered to evaluate stress distribution formulation and determine stress field in the particle. The stress profile was used to perform a crack growth analysis. The stress distribution formulation was validated by evaluating stress field for different elastic modulus value for lithiated silicon and comparing our inference against observations from prior experiments. The results showed lower modulus of lithiated silicon yielded results like experimental observations for nanoparticles. The size dependent fracture behavior was also observed in lower elastic modulus of lithiated silicon. We conclude that accurate mechanical characterization of lithiated silicon nanoparticle is necessary to model the failure of silicon particle and improving the mechanical properties may suppress crack growth in silicon nanoparticles during charging.

Manuscript submitted April 3, 2017; revised manuscript received July 11, 2017. Published July 25, 2017. *This paper is part of the JES Focus Issue on Mathematical Modeling of Electrochemical Systems at Multiple Scales in Honor of John Newman.*

Lithium ion Batteries (LIBs) are the leading source of energy storage in the electronic devices and electrical vehicles.[1] Since the development of first commercial LIBs by Sony in 1991, there has been a paramount research and development related to this battery sector. The batteries started with a graphite anode and a lithium oxide of a transition metal (specifically cobalt) as cathode.[2] Recent experimental and theoretical research has focused on identification and utilization of next generation electrode materials such as silicon in order to achieve higher energy density, longer cycle life and safer operation.[3] Silicon nanosphere and nanowire have shown extreme energy storage capacity (around 4200 mAh/g for $Li_{15}Si_4$). This high-energy storage capacity of silicon occurs due to its ability to bind up to four lithium atoms for each silicon atom. The accommodation of the large volume expansion associated with lithiation results in significant stresses in the electrode particle causing its capacity to fade over a few cycles.[4]

A lithium silicon battery system schematically shown in Figure 1a stores and discharges electrical energy through the exchange of lithium ions between the electrodes. The cell charges with lithium ions moving out of the cathode (metal oxide of lithium) and reacting with crystalline silicon at the anode to form amorphous lithiated silicon.

$$LiMO_2 \xrightarrow{Cathode} Li_{1-x}MO_2 + xLi^+ + xe^- \quad [1]$$

$$xLi^+ + xe^- + Si \xrightarrow{Anode} Li_xSi \quad [2]$$

The lithiation of nanoparticles in the silicon anode is schematically represented in Figure 1b. During the first cycle, lithiation process causes the crystalline silicon nanoparticle to convert into amorphous lithiated silicon ($Li_{15}Si_4$). Lithiation initiates with the formation of lithiated silicon amorphous shell on the crystalline silicon nanoparticle. The diffusion of lithium is very slow through the crystalline silicon, hence the phase boundary separating the crystalline core from amorphous shell is extremely sharp (~1 nm).[5] As the lithium diffuses into the particle, the reaction front propagates forward. The surface is assumed to have the highest concentration of lithiated silicon ($Li_{4.4}Si$) while the reaction front has the lowest in the lithiated domain (minimum of $Li_{3.75}Si$). The lithium concentration drops sharply in the reaction zone which is negligibly thick with no lithium in the crystalline silicon core.[6] Lithiation of the particle proceeds through progression of the sharp front along the radial direction toward the center and conversion of the nanoparticle from crystalline silicon to amorphous lithiated silicon.

Over the past decade, several theoretical models have been developed to predict the critical particle size for silicon.[7] One of the earliest work on fracture analysis of silicon bilayer was done by Huggins and Nix[8] in which they have established the critical dimensions for silicon bilayer based on linear-elastic mechanics. Two significant work by Zhao et al.[9,10] model lithiation of silicon considering a single and

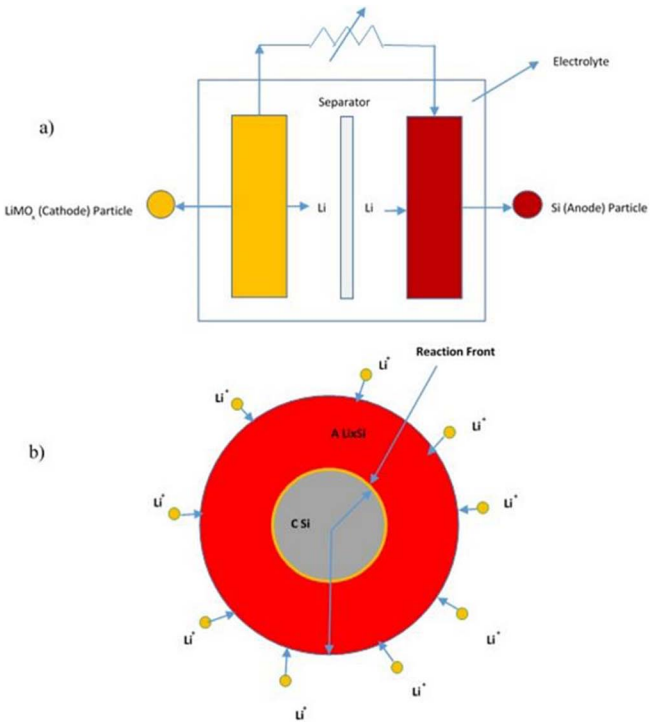

Figure 1. a) Schematic of lithium-silicon battery. b) Diffusion-Reaction Mechanism of lithium during charging in silicon nanoparticle.

[z]E-mail: shrotriy@iastate.edu

two-phase model. In their two-phase model, they have considered a plastic deformation formulation during lithiation assuming a higher elastic modulus (35 GPa) and ignoring the elastic domain due to its negligible thickness.[10] Previous approaches[10,11] toward mechanical analysis of silicon lithiation have either assumed a perfectly plastic material or elastic perfectly plastic material behavior for amorphous lithiated silicon in order to analyze the stresses due to massive volume expansion during lithiation. Ryu et al.[12] and Yao et al.[13] performed experimental and mathematical analysis based on elastic deformation to infer the critical size of silicon nanoparticle between 300–400 nm. Several different mechanical properties have been considered to mathematically model lithiation of silicon and have led to contradicting inferences. Xie et al.[14] and Zhao et al.[9] have modeled the mechanical stresses in lithiated silicon with a modulus assumption of 80 GPa and flow stress of 1 GPa for silicon nanowires. Such high modulus assumption for silicon might have been based on brittle nature of crystalline silicon. Sethuraman et al.[15] and Zhao et al.[10] reported 35 GPa as the biaxial elastic modulus for amorphous silicon. The consideration of high elastic modulus and perfectly plastic material works well for brittle materials. However, the mechanical behavior of amorphous lithiated silicon is not well understood. Recent nanoindentation tests on amorphous silicon nanowires have reported an elastic modulus within 8–12 GPa.[16] While experiments based on tensile testing reveal the flow stress between 500–750 MPa.[17] Such low elastic modulus values represent a softer, polymer-like, elasto-plastic behavior of silicon when it gets lithiated. As a step toward designing of advanced energy systems, it is important to develop a mathematical formulation for stress analysis in lithiated silicon nanoparticles which encompasses a three-layer (two-phase) model. The model needs to incorporate the crystalline silicon core which has no lithium diffusion and an amorphous shell of lithiated silicon with elastic-plastic behavior. It is necessary to understand how the mechanical properties of amorphous phase can influence the stress fields and fracture behavior of silicon nanoparticles during lithiation.

In this paper, we formulated the stress field for a two-phase silicon particle based on elasto-plastic chemo-mechanical model. We reported the influence of mechanical properties on stress and fracture analysis of silicon nanoparticles during lithiation. Stress field associated with lithiation of silicon nanoparticle was modeled using reaction driven diffusion equation. Calculated stress field was utilized to determine the driving forces for an initial radial crack in the nanoparticle. Mechanical behavior of crystalline silicon was modeled as elastic while amorphous lithiated silicon was modeled as an elastic perfectly plastic material. Numerical inferences from our model for high and low elastic modulus were compared and validated with TEM imaging results reported by Liu et al.[18] and FEM analysis by Lee et al.[19] Model predictions were used to identify the critical particle radius for fracture and to identify a mechanism for improvement of the mechanical performance of the battery.

Mathematical Modeling

Lithium transport in the silicon nanoparticle was modeled based on the following assumptions: 1) Steady state diffusion in amorphous shell, 2) Negligible diffusion in the crystalline core, 3) Sharp concentration change at the reaction front thickness, 4) Linear decay of surface lithium concentration as the reaction front penetrates the particle,[14] 5) Traction free particle expansion on the surface. The diffusion of lithium in the amorphous shell is governed by Fick's Second Law of diffusion.

$$\frac{D}{r^2}\frac{\partial}{\partial r}\left(r^2\frac{\partial c}{\partial r}\right)=0 \qquad [3]$$

Where, D is the diffusivity of lithium in amorphous silicon shell, c is the lithium concentration in the amorphous shell. To solve for steady state, the surface of silicon was initially considered to be at maximum concentration followed by a linear decay of the surface concentration as the lithium reaction front penetrated the crystalline silicon particle. The following two boundary conditions were considered to solve Equation 3.

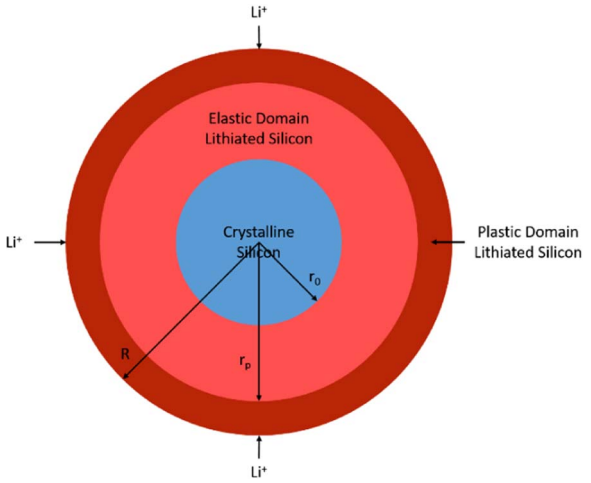

Figure 2. Schematic of stress domain in partialy lithiated silicon particle battery.

$$-D\left.\frac{\partial c}{\partial r}\right|_{r=R}=J_b \qquad [4]$$

$$c|_{r=R}=c_b=c_{\max}-y(c_{\max}-c_0) \qquad [5]$$

$$y=\frac{R-r_0}{R} \qquad [6]$$

Where, J_b is the surface flux of lithium ion, y is the relative location of the reaction front with respect to the particle surface which changes from 0 to 1, R is the particle radius, r_0 is the crystalline silicon radius and c_{max} is the maximum lithium concentration possible during lithiation of a silicon particle. The reaction is carried forward by the reaction of lithium with crystalline silicon at the reaction front. A mass balance was satisfied across the boundary of the reaction front.

$$-D\left.\frac{\partial c}{\partial r}\right|_{r=r_0}=k(c|_{r=r_0}-c_0) \qquad [7]$$

Where, k is the rate of reaction, $c|_{r0}$ is the concentration of lithium at the reaction front and c_0 is the minimum possible concentration of lithium in amorphous silicon (at the reaction front).

The concentration profile of lithium in silicon nanoparticle and the flux was obtained by solving Equation 3 using the boundary conditions (Equations 4–7). We formulated a piecewise function for the concentration that was dependent on the location of the reaction front.

$$c=\begin{Bmatrix}0; & r\le r_0\\ c_b-\frac{J_bR}{D}\left(\frac{1-r}{r}\right); & r>r_0\end{Bmatrix} \qquad [8a]$$

$$J_b=\frac{k\,(C_{max}-C_0)(1-y)}{\frac{1}{(1-y)^2}+\frac{kR}{D}\frac{y}{1-y}} \qquad [8b]$$

An elastic perfectly plastic stress model was solved to determine the stress field generated due to the lithium concentration gradient in the particle. Figure 2 represents the stress domain representation of the silicon nanoparticle. The particle was divided into three zones, i.e. crystalline core (under no equivalent stress), elastic lithiated silicon and plastic lithiated silicon. The elastic part was driven by expansion stresses due to lithium diffusion in amorphous silicon. When the yield criterion was attained, perfect plasticity was assumed to account for the plastic deformation of the electrode particle. Stress field in the particle satisfied the stress equilibrium equation.

$$\frac{\partial\sigma_r}{\partial r}+2\frac{\sigma_r-\sigma_\theta}{r}=0 \qquad [9]$$

Where σ_r and σ_θ are the radial and hoop stress in the spherical particle. In the elastic domain, the radial and hoop strain produced were calculated based on the volumetric expansion due to lithium diffusion.

$$\varepsilon_r|^{el} = \frac{1}{E}\left[\sigma_r - 2\nu\sigma_\theta\right] + \frac{\widetilde{c}\Omega}{3} \quad [10]$$

$$\varepsilon_\theta|^{el} = \frac{1}{E}\left[(1-\nu)\,\sigma_\theta - \nu\sigma_r\right] + \frac{\widetilde{c}\Omega}{3} \quad [11]$$

Where, $\widetilde{c}$ is the concentration difference with respect to lithium concentration. The yield criterion was used to establish the plastic domain based upon the yield stress of lithiated silicon (σ_y).

$$|\sigma_\theta - \sigma_r| \le \sigma_y \quad [12]$$

The three domains within the silicon particle (Figure 2), required two boundary conditions to maintain continuum and a free expansion condition for the particle. The following boundary conditions were used to merge the free expanding core to the elastic (el) domain and the latter with the plastic (pl) domain.

$$\left.\frac{\partial\sigma_r^{el}}{\partial r}\right|_{r_0} = 0 \quad [13]$$

$$\sigma_r^{el} = \sigma_r^{pl}\big|_{r_p} \quad [14]$$

$$\sigma_r^{pl}\big|_R = 0 \quad [15]$$

At the reaction front (r_0), the equivalent stress (from Equation 12) was considered zero because the crystalline core expanded only due to the stress state in amorphous shell. Incorporating the zero-equivalent stress from Equation 12 into the stress equilibrium (Equation 10), we obtained the gradient of the radial stress ($\frac{\partial\sigma_r}{\partial r}$) at the crystalline core surface to be zero. The radial stress continuity was maintained across the elastic-plastic interface at $r = r_p$. We developed the stress formulation by substituting the lithium concentration profile (Equation 8) into the elastic stress formulation (Equations 9–11) and solved the combined elasto-plastic differential equation based on the boundary conditions (Equations 13–15), which yielded:

$$\sigma_r = \begin{cases} \frac{E}{(1+\nu)(1-2\nu)}\left((1+\nu)\,C_1 - 2\,(1-2\nu)\,\frac{C_2}{r_0^3}\right) - \frac{2E\Omega}{3(1-\nu)}\frac{1}{r_0^3}\int_0^{r_0} cr^2dr; & 0 \le r < r_0 \\ \frac{E}{(1+\nu)(1-2\nu)}\left((1+\nu)\,C_1 - 2\,(1-2\nu)\,\frac{C_2}{r^3}\right) - \frac{2E\Omega}{3(1-\nu)}\frac{1}{r^3}\int_0^{r} cr^2dr; & r_0 \le r < r_p \\ -2\sigma_y \log_e\left[\frac{r}{R}\right]; & r_p \le r \le R \end{cases} \quad [16]$$

$$\sigma_\theta = \begin{cases} \frac{E}{(1+\nu)(1-2\nu)}\left((1+\nu)\,C_1 + (1-2\nu)\,\frac{C_2}{r_0^3}\right) + \frac{E\Omega}{3(1-\nu)}\left(\frac{1}{r_0^3}\int_0^{r_0} cr^2dr - c\right); & 0 \le r < r_0 \\ \frac{E}{(1+\nu)(1-2\nu)}\left((1+\nu)\,C_1 + (1-2\nu)\,\frac{C_2}{r^3}\right) + \frac{E\Omega}{3(1-\nu)}\left(\frac{1}{r^3}\int_0^{r} cr^2dr - c\right); & r_0 \le r < r_p \\ \sigma_y\left(1 - 2\log_e\left[\frac{r}{R}\right]\right); & r_p \le r \le R \end{cases} \quad [17]$$

The constants C1 and C2 were found using the radial stress boundary conditions.

$$C_1 = \frac{1}{9}(-1+2\nu)\left(\frac{\left(2c_b D{r_p}^3 + J_b R\left(R{r_o}^2 - 3R{r_p}^2 + 2{r_p}^3\right)\right)\Omega}{D{r_p}^3(-1+\nu)} + \frac{18\sigma_y \log\left[\frac{R}{r_p}\right]}{E}\right) \quad [18]$$

$$C_2 = \frac{J_b R^2 {r_o}^2 \Omega\,(1+\nu)}{18D\,(1-\nu)} \quad [19]$$

Computed stress fields were used to determine the crack driving force for radial cracks. The stress intensity factor (K_I) was calculated using the weight function theory for a semi-elliptic edge crack developed by Newman and Raju.[20] This model compared the spherical electrode particle with an equivalent cuboid having a semi-circular crack and under the same stress conditions as the particle.[20–22]

$$K_I = \frac{E}{K_{ref}(1-\nu^2)}\int_0^a \sigma_\theta(x)m(x,a)dx \quad [20]$$

$$m(x,a) = \frac{\partial}{\partial a}\left[\frac{\sigma_{\theta\max}(1-\nu^2)}{E\sqrt{2}}\left\{4F\left(\frac{a}{l}\right)\sqrt{a}\sqrt{a-x} + G\left(\frac{a}{l}\right)\frac{(a-x)^{\frac{3}{2}}}{\sqrt{a}}\right\}\right] \quad [21]$$

Where, K_{ref} is the reference stress intensity, E is the Young's Modulus, υ is the Poisson's Ratio and m is the weight function. The stress intensity factors were compared to fracture toughness (K_{1C}) of amorphous lithiated silicon.

$$K_{1C} = \sqrt{2E\gamma} \quad [22]$$

Where γ is the surface energy of the material. The governing equations were normalized to simplify the calculations.

$$\sigma_n = \frac{\sigma}{\sigma_y} \quad [23a]$$

$$r_n = \frac{r}{R} \quad [23b]$$

$$c_n = \frac{c}{c_{\max}} \quad [23c]$$

$$x_n = 1 - r_n \quad [23d]$$

$$K_n = \frac{K_I}{K_{1C}} \quad [23e]$$

The non-dimensionalized equations were solved for a silicon nanoparticle using Mathematica.[30] The mechanical and electrochemical properties listed in Table I were used to describe the crystalline silicon mechanical and lithiation response. In addition, the stress and fracture behavior were computed for three different elastic moduli of lithiated silicon as listed in Table II. First modulus corresponds to 80 GPa which has been extensively used in earlier

Table I. Silicon Properties.

Property	Value	Reference
Diffusivity, D (m^2/s)	10^{-16}	23
Reaction Rate, k (m/s)	2.54×10^{-9}	24
Maximum Concentration, c_{max} (mol/m^3)	0.36×10^6	25
Molar Volume, Ω (m^3/mol)	1.20×10^{-5}	26
Poisson's Ratio, υ	0.30	27
Surface Energy, γ (J/m^2)	0.85	28
Young's Modulus of crystalline silicon (GPa)	190.00	29
Yield Strength of lithiated silicon, σ_y (MPa)	720.00	16

Table II. Amorphous Lithiated Silicon Mechanical Properties.

	Young's Modulus, *E* (GPa)
1	80.00[9]
2	24.50[10,15]
3	12.00[16]

literature. Lithiated silicon had been considered to have a brittle nature. Second modulus value was considered based on inferences from prior Density Functional Theory calculations and experimental observations for biaxial modulus. The biaxial modulus was converted to Young's modulus using the Poisson's ratio ($E = E_{biaxial}(1 - \nu)$). The final modulus was taken as 12 GPa based on tensile and creep test observations for silicon nanowires.

Results and Discussion

The concentration profiles of lithium in the amorphous silicon shell computed for different penetration depths of the reaction front in a 200 nm particle is represented by Figure 3. The propagation of the reaction front depended on the reaction rate. The particle started with zero bulk lithium concentration at t = 0 sec. As the lithium started to react with the crystalline silicon, it moved the reaction front forward by converting it in to amorphous lithiated silicon. The crystalline and amorphous layers were separated by a sharp reaction front. The lithium diffusing into the amorphous phase from the electrolyte pushed the reaction front into the particle. As the amorphous phase expanded, it provided the saturated lithium in the outer shell more space to diffuse. This caused the slope of the concentration to gradually flatten with the increment of the reaction front. The steady state diffusion process meant that the concentration profile does not grow with time. So, the flux of lithium was not constant and reduced as the front propagated toward the center of the spherical particle.

The dimensionless stress (radial and hoop) profile was computed for the nanoparticle (radius of 200 nm) at 50% reaction corresponding to the different values of mechanical properties in Table II. The stress profiles are shown in Figures 4a, 4b and 4c for particle with 80 GPa,

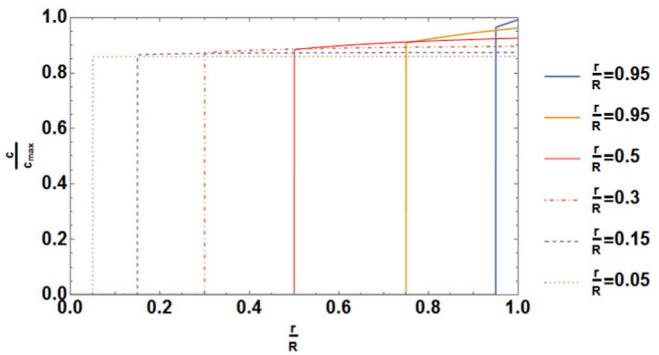

Figure 3. Normalized concentration vs normalized radius variation at different stages of penetration of reaction front into silicon particle.

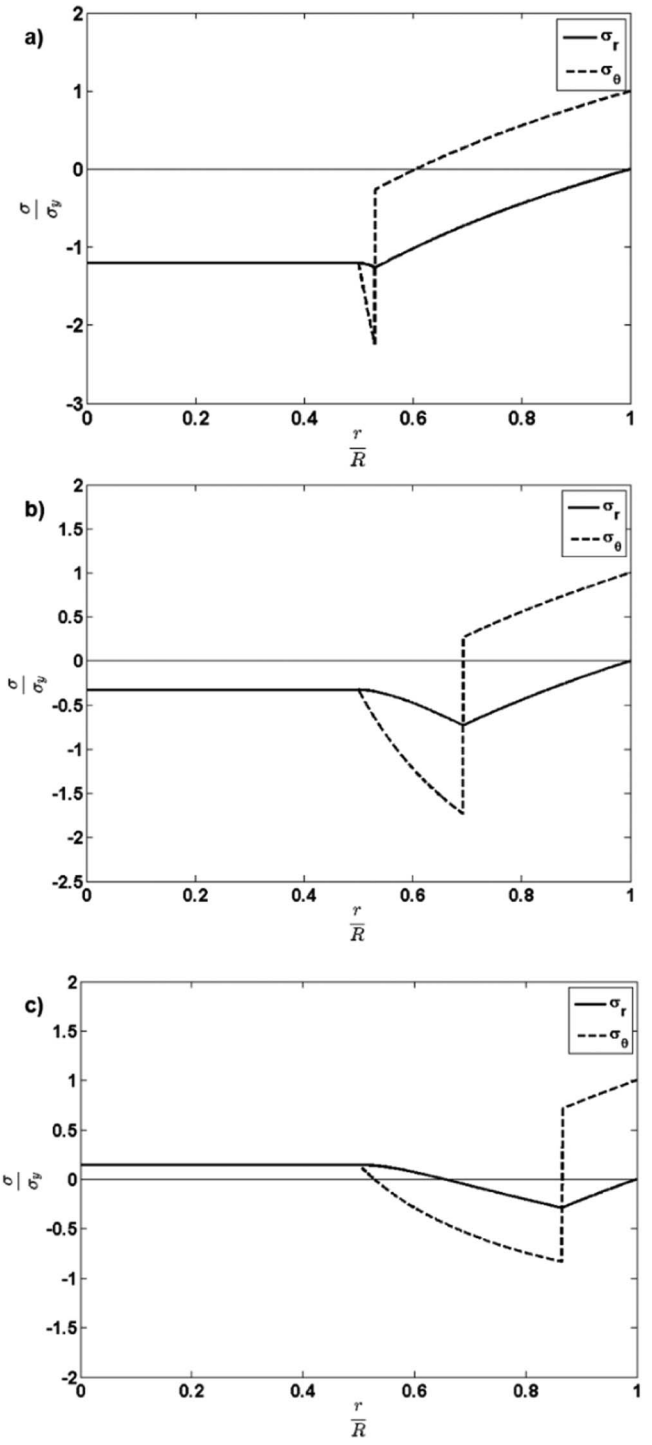

Figure 4. Normalized stress (radial and hoop) vs normalized radius (200 nm) for different elastic moduli a) 80 GPa b) 24.5 GPa c) 12 GPa.

24.5 GPa and 12 GPa, respectively. The surface of the nanosphere was considered traction free, i.e. the particle was allowed to expand freely. Due to the low diffusivity of lithium in crystalline silicon, the inner crystalline core has minimal lithium concentration. Therefore, the core has no stress gradient as it got stretched (or compressed) by the amorphous layers expanding (or contracting) during lithiation (or delithiation). In the material near the reaction front, the lithium concentration jumped and rapidly built up. The expansion due to the formation of lithiated silicon from crystalline silicon was analogous to thermal expansion and the concentration gradient across the

reaction front led to variation in the stress in the amorphous material. The elastic stresses were found compressive where the lithium concentration was higher and the stress state moved toward tension as the concentration decreased. This occurs because the higher concentration domain wanted to expand but it's free expansion was restricted by the zones with lower concentration. The particle expanded elastically until the difference between the radial and hoop stress exceeded the yield strength of the material causing plastic deformation. After the onset of yield, the material expanded through plastic deformation. As amorphous silicon was modeled as perfectly plastic, the equilibrium and yield criteria were used to determine the stress distribution in the plastically deformed zone. The stress profiles generated in Figures 4a, 4b were validated against Xie et al.[14] and Zhao et al.[10] Zhao et al.[10] have neglected the elastic domain due to its negligible thickness and only considered plastic deformation. However, the FEM analysis performed by Xie et al.[14] closely resembles the results from our formulation in Figure 4a. As shown in Figure 4, the thickness of the elastic zone increased from (a) to (c) as lower magnitude of moduli were used in the analysis. More interestingly, lower magnitude of modulus resulted in a fascinating outcome. The core silicon with higher modulus for lithiated silicon (shown in Figure 4a) was subjected to compressive stresses because the elastic domain was thin. However, for a much lower value of lithiated silicon modulus (shown in Figure 4c), the stress distribution resulted in a larger elastic domain. This led to tensile hoop stresses in both the core and the plastic domain. The development of tensile stress near the surface and core would cause any surface or internal flaws to open causing the particle to fail during charging. The crack propagation corresponding to different stress distributions was computed to better understanding the fracture of silicon nanoparticles.

An initial semi-circular flaw was considered in the particle and the computed stress intensity factors based on the stress profile in Figure 4 for different radial crack length are represented in Figures 5a, 5b and 5c. The stress intensity factors were computed for an initial radial crack emanating from outer surface and growing toward the center (based on analysis reported by Woodford et al.[21]). The tensile hoop stress in the particle resulted in opening and propagation of radial cracks. The domains having positive (or tensile) hoop stress are prone to cracking while compressive hoop stress causes crack closure and arrests the crack propagation. For Figures 5a, 5b the short cracks on the outer surface had a positive stress intensity because of positive hoop stress on the particle surface. This result was inferred by Zhao et al.[10] However, these results do not yield with the TEM results observed by Liu et al.[18] In Figures 5a, 5b, the crack grew toward the center having compressive hoop stress which causes crack closure. The deviation of the crack growth behavior for the 24.5 GPa case could be accounted for the difference in geometry. Sethuraman et al.[15] measured the biaxial modulus for a planar stress field, while the TEM results are for spherical nanowires. For the lower elastic modulus system shown in Figure 4c, the particle had tensile hoop stress both on the surface and in the core with a domain of compressive stress in the middle. This was reflected by the positive stress intensity factor on the surface (Figure 5c). The stress intensity factor became negative in a domain between the surface and core, as the compressive hoop stress caused crack closure and was positive due to the tension in the particle core. Although none of these particle cases would not fail as the K_I was less that K_{1C} in Figures 5a, 5b, 5c, but Figure 5c yielded inferences similar to experimental observations of charging induced particle fracture in in-situ TEM studies.[18] Generally, the positive stress intensity on the surface suggests that surface flaws would propagate to cause fracture. But higher compressive hoop stress in the core for higher elastic moduli would lead to surface cracks getting arrested. Experiments by Liu et al.[18] and Lee et al.[19] have shown that silicon particles above 250 nm and 350 nm, respectively, undergo complete fracture when charged. This observation suggested presence of tensile stresses both near the surface and in the core. The fracture of the particle was found to be dependent on the particle size. In addition, our results suggest that improving the moduli or hardness of the lithiated silicon may improve the fracture response during charging.

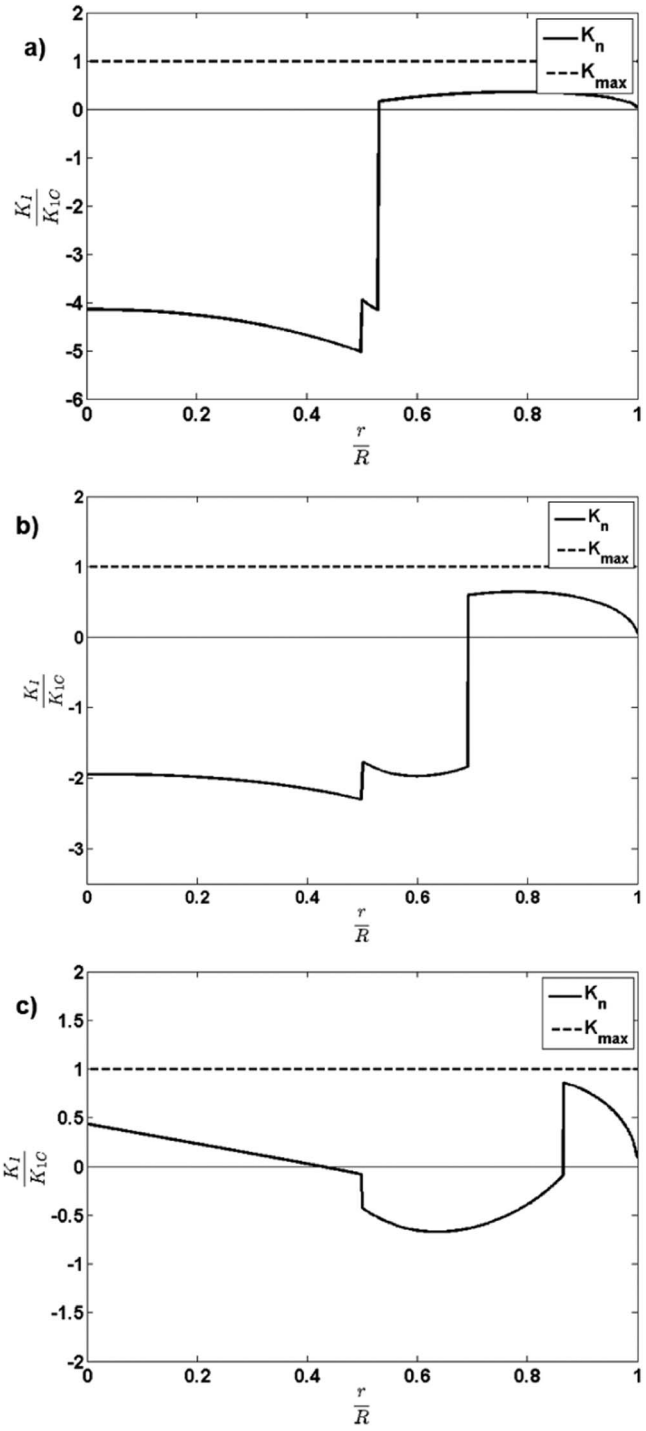

Figure 5. Normalized stress intensity factor vs normalized radius (200 nm) for different elastic moduli a) 80 GPa b) 24.5 GPa c) 12 GPa.

In order to the investigate the size dependent fracture nature of silicon nanoparticles observed by Liu et al.,[18] stress distribution and crack driving forces were computed for a particle with radius of 450 nm with a semi-circular flaw on the surface. Figure 6a shows the normalized stress state of the particle with lithiated silicon modulus of 12 GPa during charging when the reaction front had propagated half way through the material. On comparison with Figure 4c, the tensile hoop stress in the core had higher magnitude for the 450 nm particle. Figure 6b shows the normalized stress intensity for the same particle corresponding to elastic modulus of 12 GPa. The crack driving force was found greater than the fracture toughness for cracks near the core

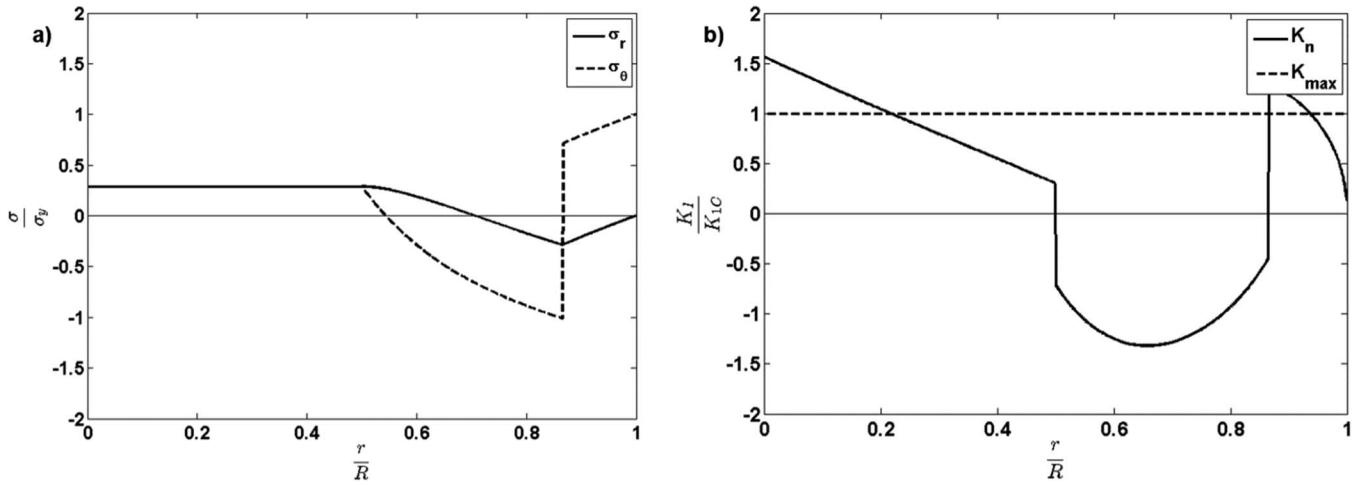

Figure 6. a) Normalized stress (radial and hoop) vs normalized radius (450 nm) for 12 GPa b) Normalized stress intensity factor vs normalized radius (450 nm) for 12 GPa.

(0.00 R ∼ 0.30 R) as well as near the surface (0.85 R ∼ 0.95 R). Presence of flaws in these zones would propagate and fail the particle. These results explained the size-dependent failure behavior of the silicon particles during charging. We conclude that particles smaller than or equal to 200 nm have lower stress distribution and thus the crack driving forces are smaller than the fracture toughness of the particle. As the particle size increases, the magnitude of charging induced stresses as well as the crack driving forces increases and thus may result in failure of larger particle (near or above 450 nm).

These results clearly showed that accurate characterization of lithiated silicon moduli is important to accurately model the stress development and cracking response of silicon nanoparticles. We suggest that increasing the modulus or hardening of lithiated silicon would improve the fracture response of silicon nanoparticles and in turn lead to designing of better energy storage materials. To test our hypothesis, we plotted the stress and stress intensity profile for the 450 nm particle having Young's Modulus of 24 GPa, i.e. twice as predicted by experiments.[16] Figure 7a shows that the elastic domain narrowed as compared to Figure 6a due to the influence of the increased elastic modulus. The narrowing of the elastic domain caused the crystalline core to have a compressive stress state. This got reflected in the stress intensity as shown in Figure 7b. The stress intensity factor due to a semi-circular crack is positive and just below the critical stress intensity near the surface (which had tensile hoop stress); and negative at the core due to compressive hoop stress. From this analysis, we conclude that an increment in the elastic modulus of the particle would allow the viable use of bigger sized silicon nanoparticles, without failure. Recent work in the field of combining silicon particles with graphene sheets allowed a mechanically and chemically stable electrode.[31] We speculate that by incorporating graphene in silicon, the volumetric expansion could be reduced leading to lower expansion stresses and the elastic modulus could be improved for better mechanical performance.

Conclusions

An elasto-plastic stress model was developed for a two-phase silicon nanoparticle during lithiation. The influence of elastic modulus and yield strength of amorphous silicon on the stress and fracture behavior of the nanoparticle was investigated. The computed stress field was utilized to understand the fracture behavior and determine the crack driving force for the growth of radial cracks present in the particle. The stress model was validated based upon the comparison among three different elastic moduli of lithiated silicon found in the literature. The numerical results indicated that predictions corresponding to lower elastic moduli (as observed from nanoindentation experiments) were able to yield with the experimentally-observed size dependence fracture of silicon particles. Our model was able to satisfy the fracture inferences drawn for high elastic

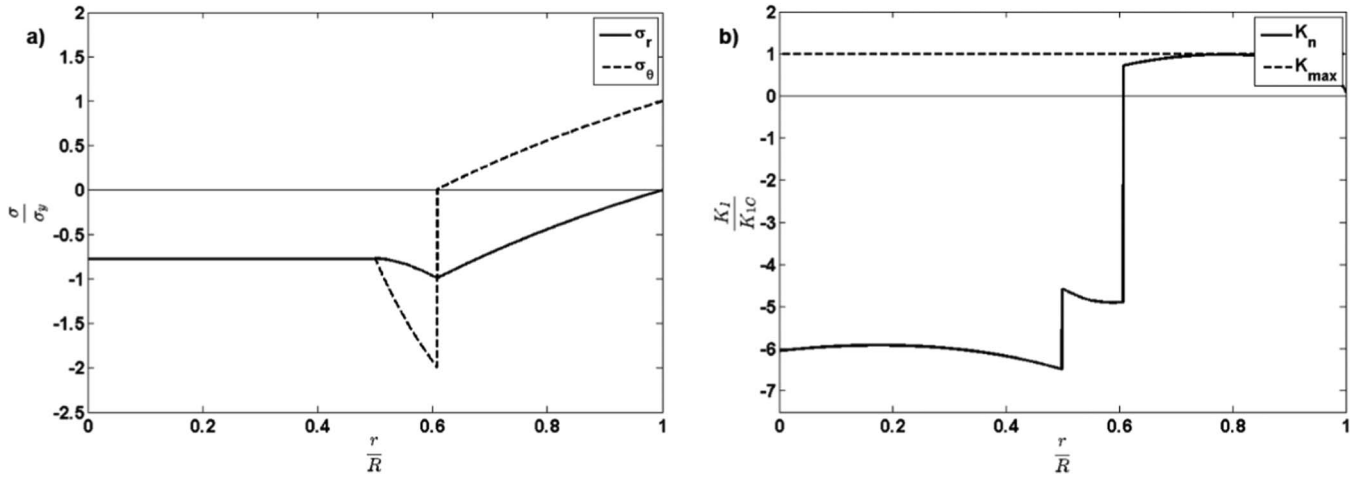

Figure 7. a) Normalized stress (radial and hoop) vs normalized radius (450 nm) for 24 GPa b) Normalized stress intensity factor vs normalized radius (450 nm) for 24 GPa.

modulus as well as capture the size-dependent particle failure observed in low elastic modulus experiments. The results showed that lower elastic modulus of amorphous silicon led to development of tensile hoop stresses in both surface and core regions of the silicon particles and thus enhanced the crack driving forces leading to their fracture. Beyond a certain critical radius (about 450 nm) a large portion of the particle was affected by stress intensity above critical value predicting failure. These results emphasized the importance of accurate characterization of the mechanical properties of amorphous lithiated silicon. Furthermore, we suggest that hardening of particle, to increase its elastic modulus, would lead to higher critical stress intensity and lower tendency to have a tensile core. This would prevent crack propagation in larger silicon nanoparticles.

References

1. M. Armand and J. M. Tarascon, *Nature*, **451**, 652 (2008).
2. M. S. Whittingham, *Chemical Reviews*, **104**, 4271 (2004).
3. B. L. Ellis, K. T. Lee, and L. F. Nazar, *Chemistry of Materials*, **22**, 691 (2010).
4. J. Chang, X. Huang, G. Zhou, S. Cui, P. B. Hallac, J. Jiang, P. T. Hurley, and J. Chen, *Advanced Materials*, **26**, 665 (2014).
5. M. J. Chon, V. A. Sethuraman, A. McCormick, V. Srinivasan, and P. R. Guduru, *Physical Review Letters*, **107**, 1 (2011).
6. L. Baggetto, D. Danilov, and P. H. L. Notten, *Advanced Materials*, **23**, 1563 (2011).
7. M. T. McDowell, S. W. Lee, W. D. Nix, and Y. Cui, *Advanced Materials*, **25**, 36 (2013).
8. R. A. Huggins and W. D. Nix, *Ionics*, **6**, 1 (2000).
9. K. Zhao, M. Pharr, S. Cai, J. J. Vlassak, and Z. Suo, *Journal of the American Ceramic Society*, **94**, 1 (2011).
10. K. Zhao, M. Pharr, Q. Wan, W. L. Wang, E. Kaxiras, J. J. Vlassak, and Z. Suo, *Journal of The Electrochemical Society*, **159**, A238 (2012).
11. M. Pharr, K. Zhao, X. Wang, Z. Suo, and J. J. Vlassak, *Nano Letters*, **10**, 1021 (2012).
12. I. Ryu, J. W. Choi, Y. Cui, and W. D. Nix, *Journal of the Mechanics and Physics of Solids*, **59**, 9 (2011).
13. Y. Yao, M. T. McDowell, I. Ryu, H. Wu, N. Liu, L. Hu, W. D. Nix, and Y. Cui, *Nano Letters*, **11**, 7 (2011).
14. Z. Xie, Z. Ma, Y. Wang, Y. Zhou, and C. Lu, *Royal Society of Chemistry*, **6**, 22383 (2016).
15. V. A. Sethuraman, M. J. Chon, M. Shimshak, N. Van Winkle, and P. R. Guduru, *Electrochemistry Communications*, **12**, 11 (2010).
16. L. A. Berla, S. W. Lee, Y. Cui, and W. D. Nix, *Journal of Power Sources*, **273**, 41 (2015).
17. A. Kushima, J. Y. Huang, and J. Li, *American Chemical Society Nano*, **6**, 9425 (2012).
18. X. H. Liu, L. Zhong, S. Huang, S. X. Mao, T. Zhu, and J. Y. Huang, *American Chemical Society Nano*, **6**, 1522 (2012).
19. S. W. Lee, M. T. McDowell, L. A. Berla, W. D. Nix, and W. Cui, *Proceedings of the National Academy of Sciences*, **109**, 4080 (2012).
20. J. C. Newman and I. S. Raju, *Engineering fracture mechanics*, **15**, 1 (1981).
21. W. H. Woodford, Y.-M. Chiang, and W. C. Carter, *Journal of The Electrochemical Society*, **157**, A1052 (2010).
22. C. Mattheck, D. Munz, and H. Stamm, *Engineering fracture mechanics*, **18**, 633 (1983).
23. Z. S. Ma, Z. C. Xie, Y. Wang, P. P. Zhang, Y. Pan, Y. C. Zhou, and C. Lu, *J. Power Sources*, **290**, 114 (2015).
24. Z. Cui, F. Gao, and J. Qu, *J. Mech. Phys. Solids*, **61**, 293 (2013).
25. L. Chen, F. Fan, L. Hong, J. Chen, Y. Z. Ji, S. L. Zhang, T. Zhu, and L. Q. Chen, *Journal of The Electrochemical Society*, **161**, F3164 (2014).
26. K. J. Zhao, W. L. Wang, J. Gregoire, M. Pharr, Z. G. Suo, J. J. Vlassak, and E. Kaxiras, *Nano Letter*, **11**, 2962 (2011).
27. S. Huang, F. Fan, J. Li, S. Zhang, and T. Zhu, *Acta Mater.*, **61**, 4354 (2013).
28. M. Tilli, T. Motooka, V. M. Airaksinen, S. Franssila, M. Paulasto-Krockel, and V. Lindaroos, *Handbook of Silicon Based MEMS Materials and Technologies*, p. 414, William Andrew (2015).
29. M. A Hopcroft, W. D. Nix, and T. W. Kenny, *Journal of the Microelectromechanical Systems*, **19**, 229 (2010).
30. Wolfram Research, Inc., Mathematica, Version 10.4, Champaign, IL (2016).
31. L. David, R. Bhandavat, U. Barrera, and G. Singh, *Nature communications*, **7**, (2016).